it becomes clear that an appropriate choice for $\boldsymbol{H}$ is a Householder transformation which satisfies

$$\boldsymbol{c}^T\boldsymbol{H} = [0, \cdots, 0, \alpha] \Leftrightarrow \boldsymbol{H}\boldsymbol{c}^* = [0, \cdots, 0, \alpha]^H. \quad (8)$$

Defining $\boldsymbol{e}_p^T = [0, \cdots, 0, 1]_{1\times p}$, we can write the Householder transformation as [12]

$$\boldsymbol{H} = \boldsymbol{I}_p - 2\frac{\nu\nu^H}{\nu^H\nu} \quad (9)$$

where

$$\nu = \boldsymbol{c}^* - \alpha^*\boldsymbol{e}_p$$

$$\alpha^* = \pm\frac{c_p^*}{|c_p|}\|\boldsymbol{c}\|. \quad (10)$$

The primary goal of $\boldsymbol{H}$ is to rotate the total energy of $\boldsymbol{c}$ into the last component, i.e., maximize $|\alpha|$ so that the norm of $x = y/\alpha$ is minimized. To accomplish this in the complex case, the phase of α must also be chosen so that $\alpha^*c_p = \alpha c_p^*$ is real [12].

For the TLS solution we only need the last column of $\boldsymbol{V}_2\boldsymbol{H} = \boldsymbol{V}_2[\boldsymbol{h}_1|\boldsymbol{h}_2|\cdots|\boldsymbol{h}_p]$ which is given by

$$\boldsymbol{V}_2\boldsymbol{h}_p = \begin{bmatrix}\alpha\\ \boldsymbol{y}\end{bmatrix}. \quad (11)$$

Since $\nu_p^* = c_p - \alpha$ and $\nu^H\nu = 2\alpha^*(\alpha - c_p)$, it is not difficult to see from (9) that

$$\begin{aligned}\boldsymbol{h}_p &= \boldsymbol{e}_p - \frac{2\nu_p^*}{\nu^H\nu}\nu\\ &= \boldsymbol{e}_p - \frac{2(c_p-\alpha)}{2\alpha^*(\alpha - c_p)}(\boldsymbol{c}^* - \alpha^*\boldsymbol{e}_p)\\ &= \frac{\boldsymbol{c}^*}{\alpha^*}. \end{aligned} \quad (12)$$

We now note that

$$\boldsymbol{y} = \frac{\boldsymbol{V}_2'\boldsymbol{c}^*}{\alpha^*} \quad (13)$$

to obtain

$$\boldsymbol{x}_{\mathrm{TLS}} = \frac{\boldsymbol{y}}{\alpha} = \frac{\boldsymbol{V}_2'\boldsymbol{c}^*}{\alpha\alpha^*} = \frac{\boldsymbol{V}_2'\boldsymbol{c}^*}{\boldsymbol{c}^H\boldsymbol{c}}. \quad (14)$$

In this form, it is easy to see that the TLS solution is identical to the noise subspace version of the minimum norm solution in [7, eq. (18)].

As pointed out in [7], the complementarity of the signal and noise subspaces allows for a signal subspace based solution. Using the partition

$$\boldsymbol{V} = [\boldsymbol{V}_1 \quad \boldsymbol{V}_2] = \begin{bmatrix}\boldsymbol{g}^T & \boldsymbol{c}^T\\ \boldsymbol{V}_1' & \boldsymbol{V}_2'\end{bmatrix} \quad (15)$$

the signal subspace version of the TLS solution is then given by

$$\boldsymbol{x}_{\mathrm{TLS}} = \frac{\boldsymbol{V}_1'\boldsymbol{g}^*}{1 - \boldsymbol{g}^H\boldsymbol{g}}. \quad (16)$$

For computational reasons, it may be advantageous to compute the TLS solution based on the smaller of the two subspaces. It is also important to realize that the TLS solutions given in (14) and (16) do not require the Householder transformation in (6) to be explicitly computed. The transformation is performed implicitly and analytically via (11).

References

[1] G. H. Golub and C. F. Van Loan, "An analysis of the total least squares problem," *SIAM J. Numer. Anal.*, vol. 17, no. 6, pp. 883–893, 1980.

[2] R. Kumaresan and D. W. Tufts, "Accurate estimation of speech-like signals," in *Proc. ICASSP*, 1982.

[3] R. Kumaresan, "Estimating the parameters of exponentially damped or undamped sinusoidal signals in noise," Ph.D. dissertation, University of Rhode Island, 1982.

[4] M. D. A. Rahman and K.-B. Yu, "Total least squares approach for frequency estimation using linear prediction," *IEEE Trans. Acoust., Speech, Signal Processing*, vol. ASSP-35, pp. 1440–1454, Oct. 1987.

[5] R. Roy and T. Kailath, "ESPRIT-estimation of signal parameters via rotational invariance techniques," *IEEE Trans. Acoust., Speech, Signal Processing.*, vol. ASSP-37, pp. 984–995, July 1989.

[6] M. D. Zoltowski and D. Stavrinides, "Sensor array signal processing via a Procrustes rotations based eigenanalysis of the ESPRIT data pencil," *IEEE Trans. Acoust., Speech, Signal Processing*, vol. ASSP-37, no. 6, pp. 832–861, June 1989.

[7] R. Kumaresan and D. W. Tufts, "Estimating the angles of arrival of multiple plane waves," *IEEE Trans. Aerosp. Electron Syst.*, vol. AES-19, no. 1, pp. 134–139, Jan. 1983.

[8] M. Kaveh and A. J. Barabell, "The statistical performance of the MUSIC and minimum-norm algorithms in resolving plane waves in noise," *IEEE Trans. Acoust., Speech, Signal Processing*, vol. ASSP-34, no. 2, pp. 331–341, Apr. 1986.

[9] K. M. Buckley and X.-L. Xu, "Spatial-spectrum estimation in a location sector," *IEEE Trans. Acoust., Speech, Signal Processing*, vol. ASSP-38, no. 11, pp. 1842–1852, Nov. 1990.

[10] Simon Haykin, *Modern Filters*. New York: Macmillan, 1989.

[11] G. H. Golub and C. F. Van Loan, *Matrix Computations*, 2nd ed. Baltimore, MD: John Hopkins University Press, 1989.

[12] C. M. Rader and A. O. Steinhardt, "Hyperbolic Householder transformations," *IEEE Trans. Acoust., Speech, Signal Processing*, vol. ASSP-34, pp. 1589–1602, Dec. 1986.

Iterative Wiener Filters for Image Restoration

Allen D. Hillery and Roland T. Chin

***Abstract*—Wiener filtering is commonly used to restore linearly degraded images. To obtain results with minimum mean-squared error, there must be accurate knowledge of the covariance of the ideal image. A set of prototype images of the ideal signal is often suggested to be used for the estimation of the covariance. However, in practical situations it is unlikely that such a set of prototypes will be available, and consequently the single copy of the degraded image is often used for the covariance estimation. This leads to undesirable restored results because of the lack of proper and sufficient images for the covariance estimate. This correspondence investigates an iterative procedure, the so-called iterative Wiener filter, which successively uses the Wiener-filtered signal as an improved prototype to update the covariance estimates. The convergence properties of this iterative filter are analyzed. It has been shown that this iterative process converges to a signal**

Manuscript received July 26, 1989; revised June 27, 1990. This work was supported by the National Science Foundation under Grants ECS-8352356 and ATM-8414467, and in part by the University of Wisconsin Graduate School research grant.

The authors are with the Department of Electrical and Computer Engineering, University of Wisconsin, Madison, WI 53706.

IEEE Log Number 9100774.

which does not correspond to the minimum mean-squared-error solution. Based on the analysis, an alternate iterative filter is proposed to correct for the convergence error. The theoretical performance of the new filter has been shown to give minimum mean-squared error. However, in practical implementation when there is unavoidable error in the covariance computation, the new filter may still result in undesirable restoration. Its performance has been investigated and a number of experiments in a practical setting were conducted to demonstrate its effectiveness.

I. Introduction

A significant amount of prior knowledge is required for the Wiener restoration filter, including knowledge of the degradation function, the covariance of the original image and of the noise [1]. Although the Wiener filter is optimally derived, its true success in restoring real-world images depends on accurate estimation of the image and noise covariances [2].

To obtain an accurate estimate of the covariances, an ensemble of many samples of the ideal image (as random variables) is required. However, in practical applications it is unlikely that there will be an ensemble of ideal image samples (that is, a set of prototype images) available for the estimation; therefore, spatial averages are often used in place of ensemble averages in implementation. To make the situation worse, in most applications only the image to be restored is available and all prior knowledge about the ideal image signal has to be estimated from it. Hence, the covariances estimated from this single copy of the degraded image are far from the true covariances of the ideal image which is required by the minimum mean-square-error estimate. For these reasons, it is expected that the restoration filter is no longer optimal because of the lack of accurate prior information.

Restoration based on other methods of estimating the required statistical information from the observed image have been suggested. For example, Chellappa and Kashyap in [3] used autoregressive and Markov image models to estimate image statistics; however, the method only works well in noise reduction and not in blur removal. Others [1], [4], [5] have proposed ways to estimate the ideal image autocorrelation from the observed image; however, a positive definite estimate has not been found and problems associated with an ill-conditioned degradation have not been addressed. Another approach, the constrained least square method, is a variant of the Wiener filter in which the autocorrelation is assumed to be of a known form [1]. In this correspondence no prototype images are assumed to be available and no restrictions are placed on the form of the autocorrelation.

By using the degraded image as a prototype an initial estimate of the signal covariance can be determined, and subsequently a restored image is obtained. It is quite plausible that this initially restored image represents a better prototype than the given degraded image, and can be used to obtain a better estimate of the covariance. This suggests an iterative procedure whereby successively restored images are used to update the covariance estimates and subsequently to improve the restoration.

This correspondence investigates issues concerning convergence and optimality of this iterative procedure. Analysis shows that the procedure converges to a fixed point which is not the minimum MSE solution. A new iterative filter is proposed to correct for the convergence error for theoretical optimal performance. However, in practical implementation, unavoidable error in the covariance computation coupled with an ill-conditioned system may cause undesirable restoration, which deviates from the theoretical optimum. Based on an error analysis, a practical procedure has been suggested to alleviate the ill-conditioned problem while producing desirable results.

Step 0: *Initialization:* Use $\mathbf{g}$ to compute an initial ($i = 0$) estimate of $\mathbf{R}_{ff}$ by

$$\mathbf{R}_{ff}(0) = \mathbf{R}_{gg} = E\{\mathbf{g}\mathbf{g}^t\}.$$

Step 1: *Filter Construction:* Use $\mathbf{R}_{ff}(i)$, the i^{th} estimate of $\mathbf{R}_{ff}$, to construct the $(i+1)^{th}$ restoration filter $\mathbf{B}(i+1)$ given by

$$\mathbf{B}(i+1) = \mathbf{R}_{ff}(i)\mathbf{H}^t[\mathbf{H}\mathbf{R}_{ff}(i)\mathbf{H}^t + \mathbf{R}_{nn}]^{-1}.$$

Step 2: *Restoration:* Restore $\mathbf{g}$ by the $\mathbf{B}(i+1)$ filter to obtain $\hat{\mathbf{f}}(i+1)$, the $(i+1)^{th}$ estimate of $\mathbf{f}$

$$\hat{\mathbf{f}}(i+1) = \mathbf{B}(i+1)\,\mathbf{g}.$$

Step 3: *Update:* Use $\hat{\mathbf{f}}(i+1)$ to compute an improved estimate of $\mathbf{R}_{ff}$, given by

$$\mathbf{R}_{ff}(i+1) = E\{\hat{\mathbf{f}}(i+1)\,\hat{\mathbf{f}}^t(i+1)\}.$$

Step 4: *Iteration:* Increment i and repeat steps 1, 2, 3, and 4.

Fig. 1. A summary of the iterative Wiener filter.

II. Iterative Wiener Restoration

The image formation model used in this paper using matrix notation (bold face symbols are used to represent vectors and matrices) is given by

$$\boldsymbol{g} = \boldsymbol{H}\boldsymbol{f} + \boldsymbol{n} \tag{2.1}$$

where $\boldsymbol{H}$ is a linear shift-invariant degradation $\boldsymbol{n}$ is an independent white noise process with known variance, $\boldsymbol{f}$ is the ideal image, and $\boldsymbol{g}$ is the observation [1]. Let us assume that we are dealing with $M \times M$ images; thus $\boldsymbol{f}$, $\boldsymbol{g}$, and $\boldsymbol{n}$ are vectors of length M^2 and $\boldsymbol{H}$ is a matrix of $M^2 \times M^2$. The Wiener solution, or linear minimum mean-square-error estimate of $\boldsymbol{f}$, denoted as $\hat{\boldsymbol{f}}$, is given by $\hat{\boldsymbol{f}} = \boldsymbol{B}$ where $\boldsymbol{B}$ is the restoration filter given by

$$\boldsymbol{B} = \boldsymbol{R}_{\mathrm{ff}}\boldsymbol{H}^t[\boldsymbol{H}\boldsymbol{R}_{\mathrm{ff}}\boldsymbol{H}^t + \boldsymbol{R}_{\mathrm{nn}}]^{-1} \tag{2.2}$$

where images are assumed to be zero mean. The solution requires accurate knowledge of $\boldsymbol{R}_{\mathrm{ff}}$, the autocorrelation of $\boldsymbol{f}$. However, in practical situations, $\boldsymbol{f}$ is usually not available and only a single copy of the blurred image to be restored $\boldsymbol{g}$ is provided. In the absence of a more accurate knowledge of the ideal image $\boldsymbol{f}$, the blurred image $\boldsymbol{g}$ is often used in its place. The signal $\boldsymbol{g}$ is subsequently used to compute an estimate of $\boldsymbol{R}_{\mathrm{gg}}$ and this estimate is used in place of $\boldsymbol{R}_{\mathrm{ff}}$ in (2.2).

As a further refinement the restored image $\hat{\boldsymbol{f}}$ has been used to provide an improved estimate of $\boldsymbol{R}_{\mathrm{ff}}$ and to repeat this process in an iterative fashion, see for example [6]. The procedure, referred to as the iterative Wiener filter, begins by using the observed image $\boldsymbol{g}$ in place of $\boldsymbol{f}$ to obtain a crude initial estimate of $\boldsymbol{R}_{\mathrm{ff}}$, then follows by restoring $\boldsymbol{g}$ to $\hat{\boldsymbol{f}}$ using (2.2). Next, the resulting $\hat{\boldsymbol{f}}$ is used to compute a refined estimate of $\boldsymbol{R}_{\mathrm{ff}}$, and subsequently a better $\hat{\boldsymbol{f}}$. This process is repeated iteratively. Fig. 1 summarizes the filtering procedure.

This iterative procedure is intuitively reasonable; in the absence of the ideal image $\boldsymbol{f}$, the filter uses the closest available image to estimate $\boldsymbol{R}_{\mathrm{ff}}$, and when a better image becomes available it is used to improve the estimate of $\boldsymbol{R}_{\mathrm{ff}}$ for restoration. However, issues of convergence still remain to be addressed.

III. Convergence of the Iterative Filter

Problems associated with convergence of the iterative restoration procedure are examined here. It remains to be shown that this iterative process converges and whether it converges to the desired Wiener solution $\hat{\boldsymbol{f}}$, which can be obtained only by knowing the true $\boldsymbol{R}_{\mathrm{ff}}$. In addition, it is important to show that error due to the estimation of $\boldsymbol{R}_{\mathrm{ff}}$ is a serious problem resulting in undesirable restoration.

We first relate the estimate of $\boldsymbol{R}_{ff}(i)$ to its subsequent improved version $\boldsymbol{R}_{ff}(i+1)$. From the update equation in step 3 of Fig. 1, we have

$$\begin{aligned}\boldsymbol{R}_{ff}(i+1) &= \boldsymbol{B}(i+1)\,\boldsymbol{R}_{gg}\boldsymbol{B}^{t}(i+1)\\ &= \boldsymbol{R}_{ff}(i)\,\boldsymbol{H}^{t}[\boldsymbol{H}\boldsymbol{R}_{ff}(i)\boldsymbol{H}^{t}+\boldsymbol{R}_{nn}]^{-1}\\ &\quad\cdot \boldsymbol{R}_{gg}[\boldsymbol{H}\boldsymbol{R}_{ff}(i)\boldsymbol{H}^{t}+\boldsymbol{R}_{nn}]^{-t}\,\boldsymbol{H}\boldsymbol{R}_{ff}^{t}(i). \qquad (3.1)\end{aligned}$$

The Wiener filter when implemented in the Fourier domain requires a circulant approximation of the block Toeplitz matrices $\boldsymbol{H}$, $\boldsymbol{R}_{ff}$, $\boldsymbol{R}_{gg}$, and $\boldsymbol{R}_{nn}$ [1]. It enables the matrices to be diagonalized by $\boldsymbol{W}$, the matrix representation of two-dimensional discrete Fourier transform. Using the circulant approximation, (3.1) can be written as

$$\begin{aligned}&\boldsymbol{W}\boldsymbol{D}_{ff}(i+1)\boldsymbol{W}^{-1}\\ &\quad= \boldsymbol{W}\boldsymbol{D}_{ff}(i)\,\boldsymbol{D}_{H}^{t}[\boldsymbol{D}_{H}\boldsymbol{D}_{ff}(i)\boldsymbol{D}_{H}^{t}+\boldsymbol{D}_{nn}]^{-1}\\ &\qquad\cdot \boldsymbol{D}_{gg}[\boldsymbol{D}_{H}\boldsymbol{D}_{ff}(i)\boldsymbol{D}_{H}^{t}+\boldsymbol{D}_{nn}]^{-t}\,\boldsymbol{D}_{H}\boldsymbol{D}_{ff}^{t}(i)\,\boldsymbol{W}^{-1} \qquad (3.2)\end{aligned}$$

where $\boldsymbol{D}_{H}$, $\boldsymbol{D}_{ff}$, $\boldsymbol{D}_{gg}$, and $\boldsymbol{D}_{nn}$ are matrices obtained by the diagonalization of $\boldsymbol{H}$, $\boldsymbol{R}_{ff}$, $\boldsymbol{R}_{gg}$, and $\boldsymbol{R}_{nn}$, respectively. Each element of the diagonalized matrices can be treated independently, permitting (3.2) to be analyzed at individual spatial frequencies independent of other frequencies. Let H, R_{ff}, R_{gg}, and R_{nn} denote the diagonal elements of the diagonal matrices $\boldsymbol{D}_{H}$, $\boldsymbol{D}_{ff}$, $\boldsymbol{D}_{gg}$, and $\boldsymbol{D}_{nn}$, respectively. For ideal autocorrelation matrices, $\boldsymbol{R}_{ff}$, $\boldsymbol{R}_{gg}$, and $\boldsymbol{R}_{nn}$ are positive semidefinite and symmetric; hence R_{ff}, R_{gg}, and R_{nn} are nonnegative and real. The element H, in general, is complex. From (3.2) we can then relate $R_{ff}(i+1)$ and $R_{ff}(i)$ in a scalar equation given by

$$R_{ff}(i+1) = \frac{R_{gg}R_{ff}^{2}(i)\,|H|^{2}}{[R_{ff}(i)\,|H|^{2}+R_{nn}]^{2}}. \qquad (3.3)$$

This relationship is valid for each element of the diagonalized matrices and $R_{ff}(i+1)$ is always real. Equation (3.3) is an update equation in that for a given starting point $R_{ff}(0)$, we can calculate successively $R_{ff}(1)$, $R_{ff}(2)$, $\cdots$.

For the iteration process to be useful, the sequence $\{R_{ff}(1), R_{ff}(2), \cdots,\}$ must converge to a fixed value $\tilde{R}_{ff}$ where it is a fixed point of the update equation, that is,

$$\tilde{R}_{ff} = R_{ff}(i+1) = R_{ff}(i). \qquad (3.4)$$

In other words, the update equation (3.3) maps $R_{ff}(i)$ into itself [7].

In order to see how the iterative filter progress with iteration, (3.3) is visualized graphically as shown in Fig. 2, where $R_{ff}(i+1)$ is plotted as a function of the variable $R_{ff}(i)$ with other parameters in (3.3) fixed at constant values. The point $\{R_{ff}(i), R_{ff}(i+1)\}$ always lies on the curve of (3.3). A diagonal line is included in the plot; where this line intersects with the curve a fixed point of (3.3) is found, that is, a point that satisfies the condition given in (3.4).

Solving for the fixed points of (3.3) yields three points given by

$$\tilde{R}_{ff} = \frac{1}{2}\left[R_{ff} - \frac{R_{nn}}{|H|^{2}} \pm \sqrt{R_{ff}^{2} - \frac{3R_{nn}^{2}}{|H|^{4}} - \frac{2R_{nn}R_{ff}}{|H|^{2}}}\right] \quad \text{and } \tilde{R}_{ff} = 0. \qquad (3.5)$$

In addition to the above graphical illustration of the fixed-point convergence of (3.3), a formal proof of the convergence can be found in the Appendix.

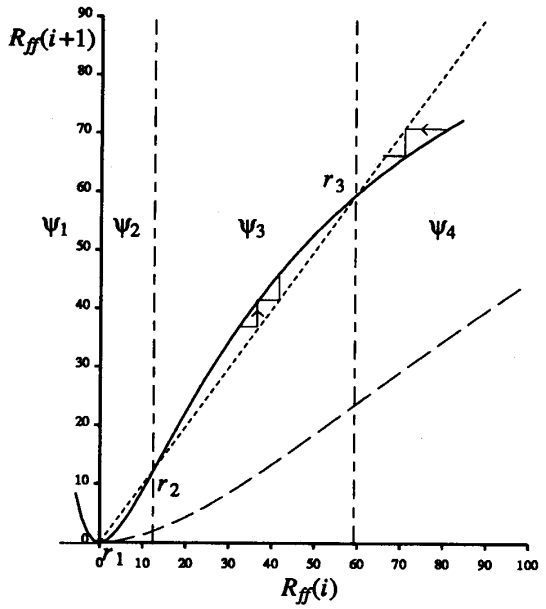

Fig. 2. Iteration of the Wiener filter. The solid curve is the plot of the update equation (3.3) for fixed $|H| = 0.19$, $R_{nn} = 1$, and $R_{ff} = 100$. The diagonal dotted line represents $R_{ff}(i) = R_{ff}(i+1)$. The two lines intersect at r_1, r_2, and r_3, which are fixed points of the iteration. For $R_{ff}(i) \in \psi_2$ the iterative procedure will always move towards $\tilde{R}_{ff} = 0$, while $R_{ff}(i) \in \psi_3$ and $R_{ff}(i) \in \psi_4$ will always move towards the leftmost fixed point, r_3. The lower dashed curve represents the update equation (3.3) when the fixed points given in (3.5) become complex; in this case the curve lies entirely below the diagonal line and the only fixed point is $\tilde{R}_{ff} = 0$.

The iterative restoration converges to either one of the two possible fixed points. If the initial guess $R_{ff}(0)$ is in region ψ_2, say, for example, close to zero, the process will converge to $\tilde{R}_{ff} = 0$, which will force the particular frequency component of the restored image to zero. Otherwise, the process will converge to the other fixed point r_3. When the fixed-points given in (3.5) become complex, the update equation (3.3) lies entirely below the diagonal line and the only fixed point is $\tilde{R}_{ff} = 0$.

Further, examining (3.5) reveals that the only instant for the fixed-point iteration to converge to the true autocorrelation R_{ff} is when $R_{nn} = 0$, that is, there is no added noise. Even in a hypothetical case, where estimation of R_{gg} is exact, as long as $R_{nn} \neq 0$, the iterative restoration will not converge to the desired minimum MSE solution.

IV. Iterative Wiener Filter: Additive Correction

It is desirable to modify the iterative process such that it converges to the true value $\boldsymbol{R}_{ff}$. The following derivation assumes that the covariance estimate is exact. One possible modification is to add a correction term to $\boldsymbol{R}_{ff}(i+1)$ given by

$$\text{Step 3':} \quad \boldsymbol{R}_{ff}^{+}(i+1) = \boldsymbol{R}_{ff}(i+1) + \boldsymbol{S}(i+1) \qquad (4.1)$$

where $\boldsymbol{S}(i+1)$ is the correction function. The correction is applied following step 3 of the iterative procedure defined in Fig. 1. The result $\boldsymbol{R}_{ff}^{+}(i+1)$ is used in place of $\boldsymbol{R}_{ff}(i+1)$ in step 1 to construct the restoration filter $\boldsymbol{B}(i+1)$. Its intention is to correct for the error resulting in step 3, which uses the restored image $\hat{f}$ instead of the ideal image f for the estimation of $\boldsymbol{R}_{ff}(i+1)$.

The additive correlation factor $S(i+1)$ is determined by expanding the update equation given by (3.1) and solving for S at the fixed point where $R_{ff}^{+}(i+1) = R_{ff}^{+}(i) = R_{ff}$ given by

$$S(i+1) = R_{ff}^{+}(i)\,[I - [B(i+1)H]^{t}]. \tag{4.2}$$

It can easily be verified that this additive correction $S(i+1)$ does lead to the ideal value R_{ff} which is a fixed point of the resulting iterative process. Substituting in the correction term and again using circulant approximation yields a new update equation. The fixed points of the update equation are determined by solving the roots at $R_{ff}^{+}(i+1) = R_{ff}^{+}(i)$ or, equivalently, by solving for the roots of the following iteration step size equation given by

$$R_{ff}^{+}(i+1) - R_{ff}^{+}(i) = \frac{|H|^2 R_{ff}^{+2}(i)\,[R_{gg} - |H|^2 R_{ff}^{+}(i) - R_{nn}]}{[|H|^2 R_{ff}^{+}(i) + R_{nn}]^2}. \tag{4.3}$$

To investigate the effectiveness of the additive correction, a proof of convergence is presented in the Appendix and the following cases are considered:

$H \neq 0$: In the case when H is not equal to or near zero, there are two fixed points at

$$\tilde{R}_{ff} = \frac{R_{gg} - R_{nn}}{|H|^2} = R_{ff} \quad \text{and} \quad \tilde{R}_{ff} = 0. \tag{4.4}$$

Any positive starting point will converge to the ideal value R_{ff}.

$H \approx 0$: In the case in which H is near singular and not equal to zero, the iteration process, after a large number of iterations, will converge to the fixed points given by (4.4). Further examination of the iteration step size in (4.3) reveals that the near-zero value of $|H|^2$ on the right-hand side equation gives rise to very small iteration step size $R_{ff}^{+}(i+1) - R_{ff}^{+}(i)$. Hence, under the near singular condition the rate of convergence is extremely slow. If the iteration process is terminated after a modest number of iterations, the well-conditioned components of H will converge to the ideal values and the ill-conditioned components will be left near their initial values.

Practical Limitations: The above analysis has used the assumption that the autocorrelation computations is exact, which is difficult to achieve practically. Implementation error due to the estimation of the covariance are unavoidable [8] and the performance of the iterative filter is strongly influenced by the accuracy of the estimate.

It is easy to see from (4.4) that for a small, nonzero value of $|H|^2$ any error in estimates of R_{gg} or R_{nn} will be significantly amplified, thus resulting in undesirable restoration results. In other words, the perturbation in the fixed point of the iteration is unbounded as $|H|^2$ tends toward zero, for any nonzero error in the covariance estimates. A complete analysis of such estimation error can be found in [9] showing that the proposed filter is sensitive to the degradation function. However, the filter has an extremely slow convergent rate which alleviates problems associated with small eigenvalues of H by early termination of the iteration.

V. Experiments

Experiments were performed to evaluate 1) the original iterative filter, and 2) the proposed correction. Test images g were generated by degrading an ideal image f using various ill-conditioned linear shift invariant blurring functions H and additive signal independent white noise n at various SNR's. The two filters were applied to restore each of the test images g. In all cases, the single copy of the degraded image was assumed to be the only available image for the covariance estimation and an unwindowed periodogram spectral estimation method was used to estimate the required covariance.

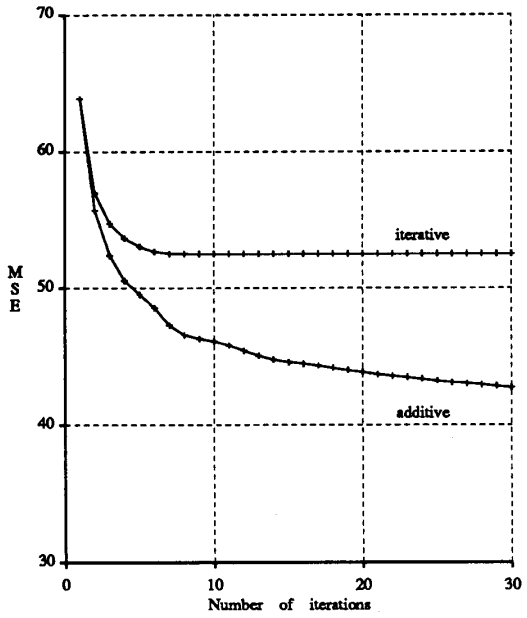

Fig. 3. Mean-square error between the ideal and restored images versus the number of iterations. The original iterative filter and the additive correction are plotted. The image degraded by an ill-conditioned H and a 40-dB SNR has an initial MSE = 145. The additive correction restored the image with substantial MSE improvement. It is to be noted that due to unavoidable error in covariance computation the additive correction method will eventually converge to a large MSE after a very large number of iterations. However, after 500 iterations, its MSE will remain at the similar low level.

The mean-square error (MSE) between f and $\hat{f}(i)$ was computed for comparison purposes and plotted as a function of iteration, as shown in Figs. 3 to 5. This error measurement denotes the aggregate error of all frequency components of the restored image. The leftmost point in each of the plots (i.e., $i = 1$) represents the result of the one-step Wiener filter, using only g as a prototype. MSE values below this $i = 1$ point represent iterative improvement, while values above it represent inferior performance.

A. Low Noise Levels

A 128 × 128 image was degraded by a linear shift invariant filter H and additive signal independent white noise. The function H was implemented as a 7 × 7 low-pass filter with uniform weights of 1/49, and the random noise was set at SNR = 30 and 40 dB. The iterative filter produced notable improvement over the one-step Wiener filter, and the additive correction produced still better results. See Figs. 3 and 4 for the MSE plots of low-noise images.

Because of the limited number of iterations applied in our experiments, it should be noted that the additive correction has not converged to a final fixed point corresponding to a bounded but large MSE measure; this large MSE measure, which deviates from the theoretical optimum, is due to error in the covariance estimates. However, it takes several thousand iterations to reach that fixed point and within the initial 100 iterations its MSE measure remains

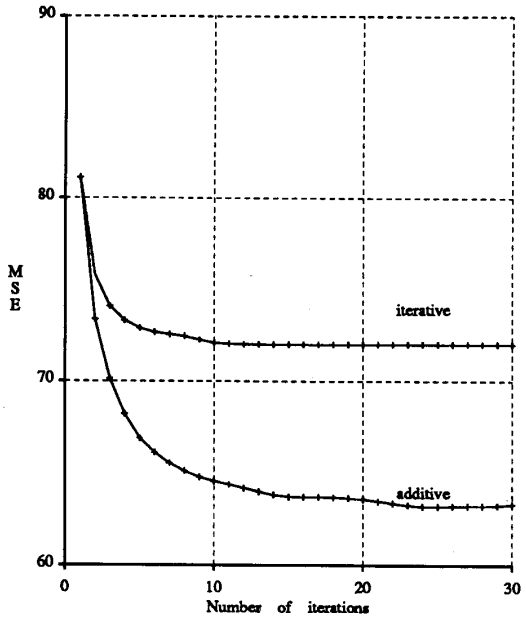

Fig. 4. Mean-square error between the ideal and restored images versus the number of iterations. The image degraded by an ill-conditioned $\boldsymbol{H}$ and a 30-dB SNR has an initial MSE = 146. The behavior of the two filters are similar to those in Fig. 3. After 200 iterations the MSE of the additive correction exceeds that of the one-step Wiener filter.

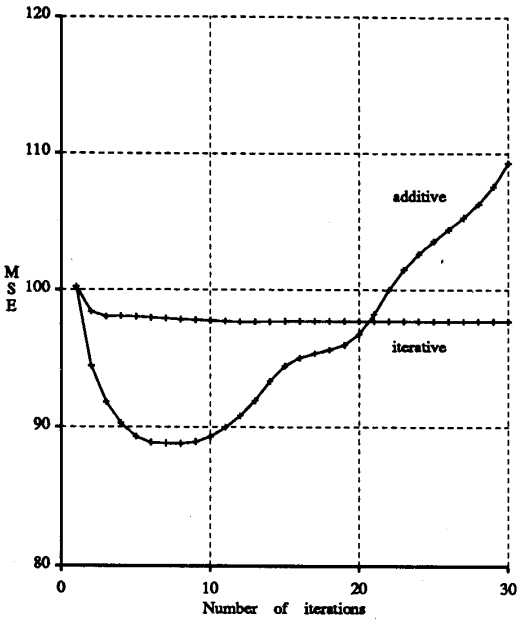

Fig. 5. Mean-square error between the ideal and restored images versus the number of iterations. The image degraded by an ill-conditioned $\boldsymbol{H}$ and a 20-dB SNR has an initial MSE = 152. After 20 iterations the MSE of the additive correction starts to increase.

relatively constant below that of the original iterative filter, making it practically useful. In one case, at 40 dB, the resulting MSE was still lower than that of the original iterative filter after 1000 iterations.

B. High Noise Levels

At low SNR, both filters did not perform well. Iterating the Wiener filter did not show much, if any, improvement over the tradi-

Fig. 6. (a) Image degraded by an 11 × 11 ill-conditioned low-pass filter and a 40-dB SNR; MSE = 674. (b) Image restored by the one-step Wiener filter, MSE = 328. (c) Image restored by 25 iterations of the iterative Wiener filter; MSE = 277. (d) Image restored by 25 iterations of the additive correction method; MSE = 236.

tional one-step Wiener filter, while the additive correction yielded large error after a brief initial moderate improvement. See Fig. 5 for the MSE plots of the 20 dB case. In one case, at 10 dB, both corrections yielded large MSE measures after a few iterations, and the iterative Wiener filter produced results inferior to the one-step Wiener filter.

A selected image set is presented in Fig. 6. A 256 × 256 original image $\boldsymbol{f}$ was degraded by an 11 × 11 low-pass filter, with uniform weights of 1/121, and a 40-dB noise level; the resulting degraded image $\boldsymbol{g}$ is shown in Fig. 6(a). Then the degraded image was restored by both filters. The noise power, the blurring function $\boldsymbol{H}$, and only the single copy of $\boldsymbol{g}$ are assumed to be known. The restored image $\hat{\boldsymbol{f}}$ using the one-step Wiener filter is shown in Fig. 6(b). It corresponds to the outcome of the first iteration of each of the iterative methods (the leftmost point in the MSE plots shown in Fig. 7). Fig. 6(c) contains the restored image obtained after 25 iterations of the original iterative filter. Fig. 6(d) contains the restored image obtained after 25 iterations with the additive correction. The corresponding MSE plots are shown in Fig. 7.

Similar results consistent with those described above were obtained when different image sets and different blurring functions were used. With SNR > 20 dB, the original iterative filter provided consistent improvement, and the additive correction method produced still better results.

VI. Conclusion

This correspondence investigated Wiener restoration of images in a practical setting where the only image available is the to-be-restored degraded image. The so-called iterative Wiener filter,

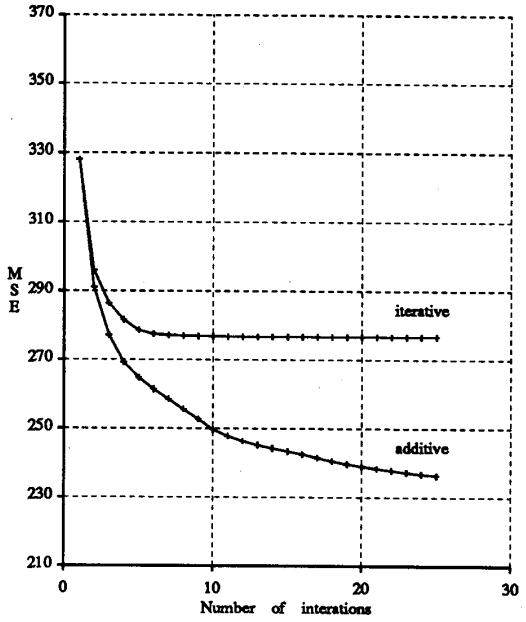

Fig. 7. Mean-square error plots of the images used in Fig. 6. The image degraded by an ill-conditioned H and a 40-dB SNR has an initial MSE = 674.

which is a procedure to circumvent the lack of prototypes of the ideal image, was analyzed and a proof of convergence was presented. However, this iterative procedure does not converge to the desired minimum MSE result, even under the ideal assumption that the imaging system is well conditioned and the covariance at each step is accurately estimated.

A correction is proposed to modify the original iterative filter for the desired theoretical minimum MSE result where exact covariance is assumed. However, in practical implementation, where there is unavoidable error in the estimation of the covariance, it has been shown that an ill-conditioned degradation would render the proposed correction ineffective. Some form of regularization is required to accommodate for ill-conditioned degradation if it is to be any use. It has been shown that the proposed correction method converges very slowly. Therefore, when terminated after a modest number of iterations, it provides a practical solution to the ill-conditioned problem while achieving desirable results. It is a subject of on-going research to determine the required number of iterations; however, experiments have shown that the restoration is insensitive to a wide range of numbers of iterations.

Appendix
Convergence Proof of the Iterative Filter

To prove the convergence of the so-called iterative Wiener filter, it is necessary to show that the update equation given by (3.1) converges to one of the fixed points. Under the circulant approximation, each of the matrices in (3.1) is diagonalized; therefore, it suffices to show that each of the independent eigenvalues given in (3.3) converge to a fixed value $\bar{R}_{ff} = R_{ff}(i) = R_{ff}(i+1)$.

For notational convenience, let

$$\{x_0, x_1, x_2, \cdots, x_i, \cdots,\} = \{x_i \mid x_{i+1} = f(x_i),\ i = 0, 1, 2, \cdots,\} \quad \text{(A.1)}$$

denote the sequence $\{R_{ff}(0), R_{ff}(1), R_{ff}(2), \cdots, R_{ff}(i), \cdots,\}$ where

$$f(x_i) = \frac{R_{gg} x^2 |H|^2}{[x_i |H|^2 + R_{nn}]^2} \quad \text{(A.2)}$$

is the sequence generating function equivalent to (3.3).

To prove the convergence of the iterative Wiener algorithm using fundamental properties of real numbers, the sequence of estimates $\{x_i \mid x_{i+1} = f(x_i),\ i = 0, 1, 2, \cdots,\}$ must be shown to be monotone and bounded [10].

Lemma: Given a continuous real-valued function f: $\boldsymbol{R} \rightarrow \boldsymbol{R}$, a starting point x_0 *member* $\boldsymbol{R}$ and a sequence $\{x_i\} = \{x_i \mid x_{i+1} = f(x_i),\ i = 0, 1, 2, \cdots,\}$. The sequence $\{x_i\}$ is monotone if $(\partial f(x)/\partial x) > 0$ for all x *member* $\boldsymbol{R}$.

Proof of Lemma: A proof by contradiction is fairly straight forward to construct using the mean value theorem, and is left as an exercise for the reader.

First let us show the sequence in (A.1) is monotone. Since R_{nn}, R_{gg}, and $|H|^2$ are real, positive numbers, $f(x)$ in (A.2) will map real, positive values of x into real, positive $f(x)$. Let us take the derivative of $f(x)$ with respect to x given by

$$\frac{\partial f(x)}{\partial x} = \frac{2x R_{nn} R_{gg} |H|^2}{[x|H|^2 + R_{nn}]^3} \geq 0.$$

Hence, using the above Lemma the sequence generated by the update equation specified by (A.1) and (A.2) with a positive starting point is monotone (either increasing or decreasing).

It is easily seen that provided the starting point is positive, the sequence $\{x_i\}$ in (A.1) and (A.2) is bounded from below by zero. This is a direct consequence of the fact noted above that $f(x)$ maps positive values of x to positive values of $f(x)$, and hence negative $f(x)$ does not exist.

Finally, to prove the monotone sequence $\{x_i\}$ is bounded from above, it suffices to show that given any real number x' greater than some known finite fixed value that the monotone sequence is decreasing, that is $f(x') < x'$. To show that all elements of the sequence $\{x_i\}$ are smaller than x', let us substitute x' into (A.2) and rewrite it to

$$f(x') = x' \frac{x'|H|^2}{x'|H|^2 + R_{nn}} \cdot \frac{r_{gg}}{x'|H|^2 + R_{nn}}.$$

For any positive values of x' and R_{nn}

$$f(x') \leq x' \frac{R_{gg}}{x'|H|^2 + R_{nn}}.$$

Furthermore, if x' is greater than the finite fixed value R_{ff}, it is clear that $R_{gg} = R_{ff}|H|^2 + R_{nn} < x'|H|^2 + R_{nn}$, and hence $f(x') < x'$.

Having shown that the sequence $\{x_i\}$ is monotone and bounded, this guarantees that a limit exists for this sequence of real numbers; therefore the iterative filter converges.

The sequence generating function for the iterative filter with the additive correction also has a nonnegative derivative. An analogous proof can be constructed to show monotone convergence.

References

[1] H. C. Andrews and B. R. Hunt, *Digital Image Restoration*. Englewood Cliffs, NJ: Prentice-Hall, 1977.

[2] M. I. Sezan and H. J. Trussell, "Use of *a priori* knowledge in multispectral image restoration," in *Proc. Int. Conf. Acoust., Speech, Signal Processing*, May 1989, pp. 1429–1432.

[3] R. Chellappa and R. L. Kashyap, "Digital image restoration using spatial interaction models," *IEEE Trans. Acoust., Speech, Signal Processing*, vol. ASSP-30, pp. 461-472, June 1982.
[4] T. S. Huang, *Advances in Computer Vision and Image Processing*. Greenwich, CT: JAI, 1984.
[5] R. C. Gonzales and P. Wintz, *Digital Image Processing*. Reading, MA: Addison-Wesley, 1977.
[6] R. K. Ward and B. E. A. Saleh, "Restoration of images distorted by systems of random impulse response," *J. Opt. Soc. Amer.*, vol. 2, no. 8, pp. 1254-1259, Aug. 1985.
[7] S. D. Conte and C. de Boor, *Elementary Numerical Analysis*. New York: McGraw-Hill, 1980.
[8] S. M. Kay, *Modern Spectral Estimation Theory and Application*. Englewood Cliffs, NJ: Prentice-Hall, 1988.
[9] A. Hillery and R. T. Chin, "Iterative Wiener filters for image restoration," Dep. Elec. Comput. Eng., Univ. of Wisconsin-Madison, Rep. TR-89-23, 1989.
[10] W. Rudin, *Principles of Mathematical Analysis*. New York: McGraw-Hill, 1976.

The Performance of Minimax Spatial Resampling Filters for Focusing Wide-Band Arrays

Jeffrey Krolik and David Swingler

***Abstract*—In recent research, coherent focusing of wide-band data received by a linear array of sensors has been achieved by adjusting the spatial sampling rate, or "spatially resampling" the array outputs, as a function of temporal frequency. Spatial resampling permits each wide-band source in multigroup multiple source scenarios to be represented by a rank-one model without preliminary estimates of the spatial distribution of the sources. This correspondence examines the design and performance of linear shift-variant filters for coherent wide-band processing via spatial resampling. In particular, a minimax error criterion is used to obtain realizable resampling filters and an approximate statistical analysis of wide-band spatially resampled minimum variance spatial spectral estimation is presented. Simulation results indicate that spatial resampling provides a computationally efficient means of reducing the threshold observation time required to obtain high resolution estimates of source location.**

I. Introduction

An important trend in wide-band spatial spectral estimation has been the use of low rank models for representing broad-band sources received at a sensor array [1]-[10]. In coherent signal-subspace methods [1]-[8], focusing matrices are used to align the signal subspaces associated with narrow-band covariance matrices in the receiver bandwidth. The estimated narrow-band covariance matrices are then averaged to obtain a focused covariance matrix wherein each source has a rank-one representation. As shown in [3], the resulting focused covariance matrix can be estimated with an accuracy which reflects the full time-bandwidth product of the sources. Although coherent signal-subspace methods offer a significant improvement in detection and resolution thresholds over incoherent methods [1], in "multigroup" scenarios where the sources are clustered around several widely separated directions [5], formation of the necessary focusing matrices has until recently required preliminary estimates of the source directions. In the multigroup case, preliminary source location estimates have been used to spatially prewhiten the field, thereby reducing it to the single-group situation [1], or to form rotational signal-subspace focusing matrices [5]. In recent work [6]-[8], however, techniques have been presented which can reduce each wideband source in multigroup scenarios to essentially a rank-one representation without preliminary estimates of the group locations. These methods are based on simply adjusting the spatial sampling rate, or "spatially resampling" the array outputs, as a function of temporal frequency so that broad-band sources are aligned in the spatial frequency domain.

The advantages of spatial resampling are that it can facilitate statistically stable broad-band spatial spectral estimation with minimal source location bias and relatively modest computational requirements. The spatial resampling method considered here is applied to the common problem of discriminating plane-wave sources with uniformly spaced linear array. The remainder of this correspondence is divided into three sections. In the next section, realizable finite-length linear shift-variant spatial filters for spatial resampling are obtained by minimizing the maximum normalized absolute error between finite-length and ideal filter outputs at each resampling point. In section three, broad-band minimum variance spectral estimation via spatial resampling is examined. Finally, simulations in the fourth section illustrate the performance of the spatially resampled minimum variance method in a five source limited observation time scenario.

II. Realizable Linear Shift Variant Filters for Spatial Resampling

Consider a field consisting of P broad-band plane-wave sources in the presence of diffuse ambient noise. It is assumed that the sources and background noises are statistically independent. For a discrete sensor array with $M = 2K + 1$ sensors spaced d meters apart along the x axis, let $y(m, \omega_k)$ denote the output of an element at position $x = md$ and temporal frequency ω_k. Under the assumed model, $y(m, \omega_k)$ for $\omega_l \le \omega_k \le \omega_h$, can be expressed as

$$y(m, \omega_k) = \sum_{i=1}^{P} s_i(\omega_k) e^{j\omega_k \alpha_i dm} + v(m, \omega_k) \tag{1}$$

where $s_i(\omega_k)$ and $\alpha_i = \sin(\theta_i)/c$, and θ_i are, respectively, the temporal Fourier transform, slowness, and bearing of the ith source relative to broadside, c is the propagation speed of the wavefront, and $v(m, \omega_k)$ is the noise component at the output of the mth sensor. Forming the vector of sensor outputs $Y(\omega_k) = [y(-K, \omega_k), y(-K+1, \omega_k), \cdots, y(K-1, \omega_k), y(K, \omega_k)]^T$, the narrow-band covariance matrix $R(\omega_k)$ is defined as $E\{Y(\omega_k)\ Y(\omega_k)^H\}$, where $E\{\cdot\}$ denotes the expectation operator, and superscripts T and H indicate transpose and conjugate transpose, respectively. Since the signals and noise are independent, $R(\omega_k)$ can be expressed as

$$R(\omega_k) = A(\omega_k, \alpha)\, P_s(\omega_k)\, A(\omega_k, \alpha)^H + R_v(\omega_k) \tag{2}$$

where $A(\omega_k, \alpha) = [a(\omega_k, \alpha_1), a(\omega_k, \alpha_2), \cdots, a(\omega_k, \alpha_P)]$ is the $M \times P$ source direction matrix, $a(\omega_k, \alpha_i) = [e^{-j\omega_k \alpha_i dK}, \cdots, e^{j\omega_k \alpha_i dK}]^T$ is the direction vector of the ith source, $P_s(\omega_k)$ is an un-

Manuscript received August 17, 1989; revised August 11, 1990. This work was supported by the Canadian Defence Research Establishment Atlantic, Dartmouth, N.S., under Contract W7707-7-7934.

J. Krolik is with the Department of Electrical and Computer Engineering, Concordia University, Montreal, Que., Canada H3G 1M8.
D. Swingler is with the Division of Engineering, Saint Mary's University, Halifax, Nova Scotia, Canada B3H 3C3.

IEEE Log Number 9100776.